Developmental Biology 394 (2014) 277–291

Contents lists available at ScienceDirect

Developmental Biology

journal homepage: www.elsevier.com/locate/developmentalbiology

Drosophila protein kinase N (Pkn) is a negative regulator of actin–myosin activity during oogenesis

Tânia Ferreira [a], Pedro Prudêncio [a,b,c], Rui Gonçalo Martinho [a,b,c,*]

[a] Instituto Gulbenkian de Ciência, Rua da Quinta Grande 6, Oeiras 2781-901, Portugal
[b] Departamento de Ciências Biomédicas e Medicina, Universidade do Algarve, Campus de Gambelas, 8005-139 Faro, Portugal
[c] IBB-Institute for Biotechnology and Bioengineering, Centro de Biomedicina Molecular e Estrutural, Universidade do Algarve, Campus de Gambelas, 8005-139 Faro, Portugal

ARTICLE INFO

Article history:
Received 20 June 2014
Received in revised form
8 August 2014
Accepted 9 August 2014
Available online 15 August 2014

Keywords:
Drosophila
Morphogenesis
Oogenesis
Actin–myosin
Protein kinase N

ABSTRACT

Nurse cell dumping is an actin–myosin based process, where 15 nurse cells of a given egg chamber contract and transfer their cytoplasmic content through the ring canals into the growing oocyte. We isolated two mutant alleles of *protein kinase N* (*pkn*) and showed that Pkn negatively-regulates activation of the actin–myosin cytoskeleton during the onset of dumping. Using live-cell imaging analysis we observed that nurse cell dumping rates sharply increase during the onset of fast dumping. Such rate increase was severely impaired in *pkn* mutant nurse cells due to excessive nurse cell actin–myosin activity and/or loss of tissue integrity. Our work demonstrates that the transition between slow and fast dumping is a discrete event, with at least a five to six-fold dumping rate increase. We show that Pkn negatively regulates nurse cell actin–myosin activity. This is likely to be important for directional cytoplasmic flow. We propose Pkn provides a negative feedback loop to help avoid excessive contractility after local activation of Rho GTPase.

Introduction

Force generation by the contractile actin–myosin cytoskeleton is indispensable for most morphogenetic processes (Levayer and Lecuit, 2012; Vicente-Manzanares et al., 2009). The actin cytoskeleton is a highly dynamic structure and its super-organization regulated by a large number of actin-binding proteins. After myosin regulatory light chain (MRLC) phosphorylation the myosin hexamer binds actin filaments (F-actin) and cross-links them, making the filaments slide across each other, and facilitating contractility and cortical tension (Gardel et al., 2004; Ikebe et al., 1988; Jung et al., 2008; Koenderink et al., 2009). Although the basic molecular mechanisms required for contractility and force generation are well known, the way in which they are spatially and temporally coordinated for coherent morphogenesis is still poorly understood.

Myosin is a hexamer of three different subunits: two heavy chain subunits (MRHC, zipper in *Drosophila*), two regulatory light chains (MRLC, spaghetti squash in *Drosophila*) and two essential myosin light chain subunits (Sellers, 2000). GTPases are the most common regulators of cytoskeletal reorganization and cell adhesion (Nobes and Hall, 1995; Ridley and Hall, 1992). The most prominent members of the Rho-family GTPases are RhoA, Rac1, and Cdc42. A major effector of RhoA is the serine/threonine kinase Rho-associated kinase (ROK). Rho–GTP binds to the Rho-binding domain (RBD) of ROK to release it from auto-inhibition. ROK is both directly and indirectly responsible for MRLC phosphorylation and increased contractility (Jung et al., 2008; Kimura et al., 1996; Leung et al., 1996). Levels of MRLC phosphorylation result from the equilibrium between the activities of distinct kinases (e.g., MLCK – myosin light chain kinase, ROK, and ZIP kinase – leucine zipper interacting kinase) and phosphatases (in most cases, myosin phosphatase 1) (Grassie et al., 2011; Matsumura, 2005).

Protein kinase N (PKN) belongs to a sub-group of the protein kinase C (PKC) family of kinases (Mukai, 2003; Mukai and Ono, 1994). In vertebrates there are three PKN paralogs (PKN1/PRK1, PKN2/PRK2 and PKN3/PRK3) (Mukai, 2003; Oishi et al., 1999; Quilliam et al., 1996; Vincent and Settleman, 1997). Although the precise molecular function of these protein kinases is still unknown, they have been associated with stress fiber formation, cortical actin reorganization during cell migration, regulation of cell–cell adhesion and apical junction formation, control of mitotic entry and exit from cytokinesis, and importantly, tumor progression and invasiveness (Calautti et al., 2002; Dong et al., 2000; James et al., 2013; Leenders et al., 2004; Lim et al., 2004; Mopert et al., 2012; Schmidt et al., 2007; Unsal-Kacmaz et al., 2012; Vincent and Settleman, 1997; Wallace et al., 2011).

* Corresponding author at: Departamento de Ciências Biomédicas e Medicina, Universidade do Algarve, Campus de Gambelas, Gambelas, 8005-139 Faro, Portugal.
E-mail address: rmartinho@igc.gulbenkian.pt (R.G. Martinho).

http://dx.doi.org/10.1016/j.ydbio.2014.08.008
0012-1606/

Drosophila melanogaster has only one representative of the PKN subgroup. *Drosophila* Pkn (hereafter referred to as Pkn) is important for embryonic dorsal closure (Lu and Settleman, 1999). Dorsal closure results from the movement of the lateral and ventral epidermis to enclose the *Drosophila* embryo after germ-band retraction. This involves significant cell shape changes associated with profound rearrangements of the actin–myosin cytoskeleton (Jacinto et al., 2002). In the first phase of dorsal closure, the dorsal most cells of the lateral epidermis elongate along the dorsal–ventral axis in a Rho-dependent manner. This is associated with the accumulation of actin and non-muscle myosin at the leading edge of the epithelial sheet. Pkn is required for cells to be able to maintain elongation, and embryos mutant for *pkn* show dorsal closure defects (Betson and Settleman, 2007; Lu and Settleman, 1999).

Drosophila oogenesis has an assembly line organization where progressively older egg chambers develop within an ovariole to ultimately give rise to a fully matured egg (Bastock and Johnston, 2008). The germ line stem cells asymmetrically divide within the germarium to produce a cystoblast. The cystoblast divides four more times to make a cluster of sixteen cells connected to each other by cytoplasmic bridges called the ring canals. One of these cells will differentiate as an oocyte whereas the other 15 will become the supportive nurse cells. The nurse cells produce mRNAs, proteins, and organelles that are delivered to the developing oocyte. Nurse cell dumping is an actin–myosin based process in which the 15 nurse cells of a given egg chamber contract and transfer their cytoplasmic content through the ring-canals into the growing oocyte (Mahajan-Miklos and Cooley, 1994; Wheatley et al., 1995). We observed that the transition between slow and fast dumping was a discrete event with at least a five-fold increase of cytoplasm transfer rates. We isolated two novel mutant alleles of *pkn* that showed significant defects during *Drosophila* oogenesis. We observed that Pkn behaved as a negative regulator of actin–myosin activity during the onset of fast nurse cell dumping. Egg chambers whose germ line was mutant for *pkn*, showed loss of tissue integrity and abnormally low nurse cell cytoplasm transfer rates. Both phenotypes were most likely the result of excessive contractility. Our work shows that *Drosophila* Pkn is a negative regulator of actin–myosin activity, whose function is most likely important for coordination of cellular contractility during morphogenesis. We propose Pkn provides a negative feedback loop to help avoid excessive contractility after local activation of Rho GTPase.

Methods

Fly work and genetics

Flies were raised using standard techniques. Both pkn^{1T} and pkn^{2T} alleles were isolated in a previously reported maternal screen (Pimenta-Marques et al., 2008). Maternal mutant embryos and germ line mutant clones were generated using the FLP/FRT ovo^{D} system (Chou and Perrimon, 1992).

All other lines used in this work were acquired from the Bloomington stock center, except: w; SQH::sqh-GFP and w;; SQH::sqh(T20E,S21E) (line81)/TM3Sb which were a gift from Dr. Roger Karess (Royou et al., 2004, 2002). l(3)72Dd03802/TM6B (DMBSP1, in this work referred as DMBS), was a gift from Dr. Yasuyoshi Nishida (Mizuno et al., 2002).

Mutant germ line clones were made by crossing FRT42B (mutant allele)/CyO virgin females to hs::FLP; FRT42B ovo^{D}/CyO males, and heat shocking the progeny at 37 °C for 1 h during second and third larvae instar stages. For FRT42B germ line clone controls, FRT42B/CyO virgin females were crossed to hs::FLP; FRT42B ovo^{D}/CyO males, followed by heat shock as previously described. Oregon R (OR) strain was also used as a control.

To generate homozygous mutant clones in ovaries (negatively marked for nuclear GFP), y,w, hs::FLP; FRT42B nlsGFP/CyO hs::hid virgin females were crossed with w; FRT42B, (mutant allele)/CyO males. Recombination was induced by 1 h heat shock at 37 °C during second and third instar larvae stage. Adult ovaries were harvested from 4–5 days old females, and subsequently processed for immunofluorescence.

Cloning of pkn alleles

To identify the affected gene responsible for the lethality of complementation group 8 (CG8) mutant alleles, complementation analysis was performed using the Bloomington 2R Deficiency kit. The following deficiencies failed to complement both alleles: Df (2R)G53/CyO (BL6227), Df(2R)Np3/CyO (BL258), Df(2R)w45-30n/CyO (BL4966), Df(2R)w73-1/CyO (BL6246), Df(2R)Np5,In(2LR)w45-32n/CyO (BL3591). Deficiency Df(2R)BSC29/CyO (BL6917) complemented the zygotic lethality of both alleles. This mapped both CG8 alleles to cytological interval 45A3-A13.

Three of the deficiencies (Df(2R)w45-30n/CyO, Df(2R)G53/CyO and Df(2R)w73-1/CyO) were also crossed with known recessive mutant alleles for distinct candidate genes within 45A3-A13 interval. CG8 alleles were mapped to the genetic interval between the *hikaru genki* (*hig*) and *l(2)03659* genes, which corresponds to the cytological interval between 45A6-A9.

By a candidate gene approach it was concluded that both CG8 alleles failed to complement six known lethal P-elements of *protein kinase N* (*pkn*): pkn^{3} (BL5523), pkn^{2} (BL6103), pkn^{K11209} (BL11018), pkn^{RG232} (BL12052), $pkn^{KG02139}$ (BL14584) and pkn^{06736} (BL12322). Sequencing of the genomic region associated to the *pkn* gene, confirmed that both isolated alleles contained distinct point mutations within the *pkn* open-reading frame that were expected to strongly impair Pkn protein levels. DNA polymorphisms within the *pkn* gene locus were controlled through the use of a mutant allele isolated in the same screen but that belongs to a distinct complementation group (Pimenta-Marques et al., 2008). Confirming that CG8 alleles were allelic to *pkn*, they were phenocopied by a previously isolated allele of *pkn* (pkn^{06736}) (Lu and Settleman, 1999).

Criteria used for staging of stage 9, 10A, and 10B egg chambers

Stage 9: Displacement of the border cell cluster (BCC) from the anterior follicle epithelium, and migration within the nurse cell cluster (NC) up to the contact of the posterior-most BC in the cluster to the anterior surface of the oocyte (OO) (basically encompassing BCC migration). Migration of the follicle cells (other than BC or stretch cells) simultaneously and in coordination with the BCC migration. Egg chambers with defects in BCC migration were not considered.

Stage 10A: BCC at the OO anterior surface, already with more than one BC from the cluster contacting the OO membrane. Centripetal cells (CC) aligned along the anterior OO membrane. Egg chambers whose centripetal cells had some cell shape remodeling were considered, provided migration between the NC and the OO was not initiated. Restricted cytoplasmic actin filaments polymerization. Squamous epithelium (cell-shape remodeled stretch cells) formed over the NC. Ratio between the NC and the egg chamber length bigger or equal to 0.5. Egg chambers with incomplete BCC migration were not considered.

Stage 10B: Initiation of CC migration between the NC and the anterior OO membrane to fully surround the OO. Follicle cells, other than CC and stretch cells, remodel their shape to surround the OO. Cytoplasmic/cortical actin filaments actively polymerized to anchor the NC nuclei during dumping. Ratio between the NC

and the egg chamber length smaller than 0.5. BCC at the dorsal–anterior side of the OO membrane. Egg chambers with incomplete BCC migration and/or CC migration defects were not considered.

Although morphological variations occurred even within egg chambers of similar stages, similarly looking chambers were always compared to avoid developmental differences within each stage.

Quantification of female egg laying

The total number of eggs laid by each female, per day, was scored using the following procedure: ten 1-day old germ line mutant female virgins were mated to ten 1-day old wild-type males (OR). Females were allowed to lay eggs in apple juice agar plates for consecutive 24 h periods, at 25 °C. Total number of eggs was scored and divided by the total number of living females at each time point. Three independent replica experiments were performed. The first plate in each experiment (corresponding to the first 24 h) was in each case discarded as it corresponded to a period of female maturation and matting.

Quantification of egg length

Egg length (defined here as the distance between the micropile basis and the posterior pole) was used as a measure of total egg size. 2–3 days old germ line mutant virgin females were collected and crossed with wild-type males (OR). Females were allowed to lay eggs overnight at 25 °C on apple juice agar plates. Individual eggs were imaged using a Zeiss SteREO Lumar V12 stereoscope and their individual length measured. At least three independent crosses were performed for each genotype, and at least three consecutive egg laying plates were collected for each replica. Wild-type (OR), w; FRT42B and w; FRT42B *san*/CyO (Pimenta-Marques et al., 2008) stocks were used as controls.

Quantification of ring canal inner diameter

Phalloidin-positive ring canal (RC) size was measured as a function of inner RC diameter in stage 10 egg chambers, using the 3D projection tool from Leica LAS AF Lite software.

Quantification of nurse cell to oocyte membrane breakdown

Nurse cell to oocyte membrane breakdown phenotype is defined here as the disruption of the posterior-most nurse cell (NC)/oocyte anterior-most (OO) membrane. We scored positive for membrane breakdown when we observed at least one of the following events in phalloidin positive egg chambers: (1) gaps in the integrity of the NC/OO membrane, other than ring canals, (2) ring canals within the oocyte cytoplasm, (3) border cells within the oocyte cytoplasm, or (4) nurse cell nuclei within the oocyte cytoplasm.

Quantification of cortical F-actin and myosin accumulation in the nurse cells

For F-actin measurements, phalloidin-positive stage 10 egg chambers images were taken. SQH::sqh-GFP was used for total myosin level quantification. Myosin activation was measured as a function of its specific phosphorylation in the Myosin Regulatory Light Chain subunit (MRLC or Spaghetti Squash (Sqh) in *Drosophila*). Human MRLC Thr18 and Ser19 residues correspond to *Drosophila* Sqh Thr20 and Ser21; and their phosphorylation leads to myosin activation.

1) Monophosphorylated myosin (1p-myosin). We used two different antibodies: rabbit anti-human monophosphorylated-Myosin Light Chain 2 (pSer19) (1:500, Cell Signaling, 3671) and guinea pig anti-*Drosophila* monophosphorylated SQH (pSer21) (1:100, a gift from Dr. Robert Ward).
2) Diphosphorylated myosin (2p-myosin). We used two different antibodies: rabbit anti-human diphosphorylated Myosin Light Chain 2 (pThr18, pSer19) (1:200, Cell Signaling, 3674) and rat anti-*Drosophila* diphosphorylated SQH (pThr20, pSer21) (1:1000, a gift from Dr. Robert Ward).

Quantification of accumulation phenotypes was done using three scoring classes: class 1=low accumulation, class 2=intermediate accumulation, and class 3=high accumulation. Phenotypic quantification is semi-quantitative based on confocal staining intensity and morphology. Representative examples are shown in Supplementary Fig. 6.

Immunohistochemistry

Ovaries immunostaining was performed as previously described (Guilgur et al., 2012; Pimenta-Marques et al., 2008). Briefly, 2–3 days old females were transferred overnight to food vials supplemented with live baker's yeast. Ovaries were then dissected out in ice-cold 1x PBS, pH=7.4, and immediately fixed in ice cold 1x PEMS with 4% formaldehyde and 1 mM CaCl2, for 20 min at RT with agitation. Ovaries were washed 3 × 5 min in 1 × PBS+0.2% Tween-20 (PBST-0.2%), teased apart and permeabilized with PBST-0.2%+1% Triton X-100 for 1 h at RT with agitation and blocked using PBST-0.2%+1–5% Bovine Serum Albumin (BSA) for 1 h at RT, with agitation.

Primary antibodies were incubated overnight at 4 °C, with agitation, but the incubation solution was different between antibodies:

a) PBST-0.2%+1% BSA: mouse anti-Armadillo (1:50, Armadillo N27A1, Developmental Studies Hybridoma Bank, DSHB), rat anti-DE-Cadherin (1:20, DCAD2, DSHB) and mouse anti-SQH (1:1000, a gift from Dr. Robert Ward).
b) PBST-0.2%+0.3% Triton-X100+5% BSA: rabbit anti-2phospho-Myo2 (pThr18, pSer19) (1:200, Cell Signaling, 3674), rabbit anti-phospho-Myo2 (pSer19) (1:500, Cell Signaling, #3671), rat anti-SQH-2p (pThr20, pSer21) (1:1000, a gift from Dr. Robert Ward), guinea pig anti-SQH-1p (pSer21) (1:100, a gift from Dr. Robert Ward).

Ovaries were then washed 3 × 20 min in PBST-0.2%, followed by overnight incubation with the appropriate secondary antibodies at 4 °C, with agitation. Secondary antibodies were Cy3- and Cy5-conjugated, diluted at 1:1000 (Jackson ImmunoResearch Laboratories, West Grove, PA) and Alexa488-conjugated at 1:1000 (Molecular Probes).

Wheat germ agglutinin (WGA, Alexa Fluor® 647 conjugate, Invitrogen W32466) was used for nuclear envelope staining at 1:500 in PBST-0.2% for 2 h at room temperature with rotation. For F-actin detection, rhodamine conjugated phalloidin (Sigma; 1:200 of stock concentration 1 mg/ml) was incubated for 10 min in PBST-0.2%. For DNA staining, Sytox-green was used (Life Technologies) at 1:1000 dilution with 5 μg/ml RNase A in PBST-0.2% for 30 min at room temperature.

Samples were mounted in Fluorescent Mounting Medium (DakoCytomation, Inc.) and immunostaining visualized using a Leica SP5 confocal inverted microscope.

Generation of pkn antibodies

An anti-Pkn rabbit polyclonal antibody was raised against a recombinant protein corresponding to amino acids 147-392 of

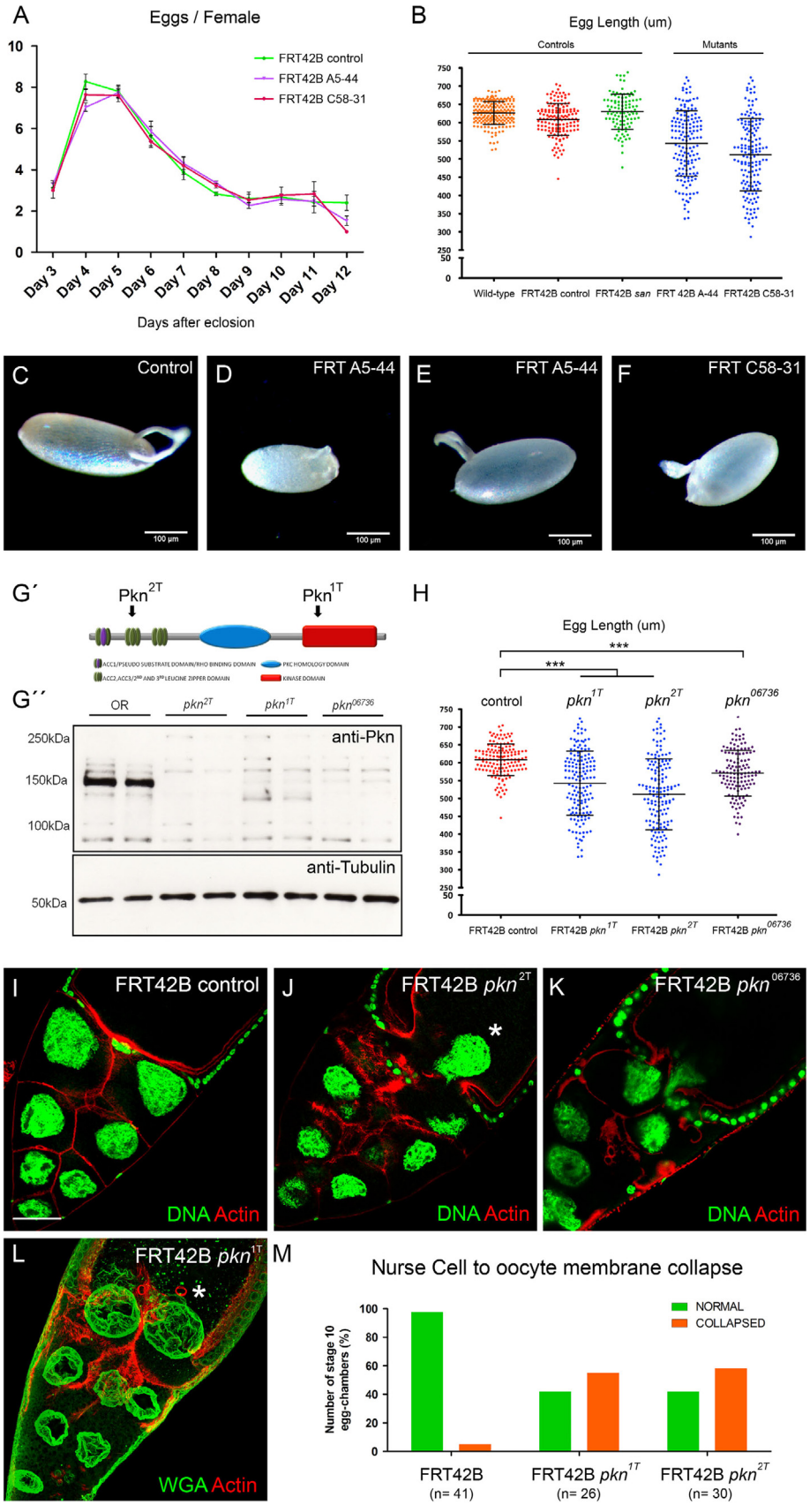
A
Eggs / Female
FRT42B control
FRT42B A5-44
FRT42B C58-31
Days after eclosion
B
Egg Length (um)
Controls
Mutants
Wild-type
FRT42B control
FRT42B san
FRT 42B A-44
FRT42B C58-31
C Control
D FRT A5-44
E FRT A5-44
F FRT C58-31
100 µm
G´
Pkn2T
Pkn1T
G´´
OR
pkn2T
pkn1T
pkn06736
250kDa
150kDa
100kDa
50kDa
anti-Pkn
anti-Tubulin
H
Egg Length (um)
control
pkn1T
pkn2T
pkn06736
FRT42B control
FRT42B pkn1T
FRT42B pkn2T
FRT42B pkn06736
I FRT42B control
J FRT42B pkn2T
K FRT42B pkn06736
DNA Actin
L FRT42B pkn1T
WGA Actin
M
Nurse Cell to oocyte membrane collapse
NORMAL
COLLAPSED
Number of stage 10 egg-chambers (%)
FRT42B (n= 41)
FRT42B pkn1T (n= 26)
FRT42B pkn2T (n= 30)

Pkn, expressed as a fusion protein with a N-terminal 10 × His tag (Metabion International AG). This region corresponds to the regulatory binding domain of Pkn.

Western blotting

Embryos were collected 0–3 h after egg laying and dechorionated with 50% commercial bleach solution for 5 min. For each sample ten embryos were ruptured with a needle in 10 ul 2 × SDS-PAGE sample buffer and heated for 5 min at 100 °C. Protein samples were run on 8% SDS-PAGE gels and proteins transferred to Hybond-ECL membranes (Amersham). Membranes were blocked overnight at 4 °C in 5% non-fat milk in PBT. Primary antibodies were added and incubated overnight at 4 °C. Following washes with PBT, HRP-conjugated antibodies were added and incubated for 2 h at room temperature. Detection was performed using ECL solution for 1 min and Hyperfilm ECL (Amersham). Primary antibodies used were rabbit anti-Pkn at 1:1000 dilution (this work), rabbit anti-aPKC at 1:2000 dilution (Santa Cruz, sc-216) and mouse anti-alpha-Tubulin Dm1A at 1:20,000 dilution (Sigma). Secondary detection was performed with rabbit and mouse HRP-conjugated antibodies at 1:4000 dilution (Jackson ImmunoResearch).

Live imaging of nurse cell dumping

hs::FLP; FRT42B SQH::sqh-GFP, *pkn*/CyO females were crossed to hs::FLP; FRT42B ovo^{D}/CyO males and left to egg lay for 24 h. F1 progeny was heat-shocked for 1 h at 37 °C at both the second and third instar. hs::FLP; FRT42B SQH::sqh-GFP, *pkn*/FRT42B ovo^{D} females were collected 1–2 days after eclosion and left for 36 h in food supplemented with live baker's yeast.

Ovaries were rapidly dissected in the dry and transferred to live imaging medium (Schneider *Drosophila* Media (GIBCO, 21720-024) supplemented with 0.2 mg/ml insulin (GIBCO, 12585-014) and 20% FBS (Sigma, F7524)). Individual egg chambers were manually separated and transferred individually to a home-made acrylic multi well plate containing fresh live imaging media (approximately 300–500 μ of media per well), in which the top and bottom are coverslips. Each well was then covered with a second coverslip. Control and mutant samples were always prepared and imaged at the same time. Images were acquired using a 20 × objective mounted on a Nikon Eclipse TE2000-S Screening Microscope. Time lapse was done every 1.7 min using the Micromanager Platform. For live-cell imaging were only used egg chambers without any detectable nurse-cell-to-oocyte membrane collapse, normal cytoplasmic streaming and normal nuclear morphology at the beginning and during data acquisition. This was assessed using DIC and/or Sqh-GFP. We used Histone2av-GFP to validate our DIC analysis of egg chambers nuclear morphology and integrity (data not shown). During imaging, transmitted light and UV channels were always used to access viability of egg chambers (e.g. nuclear morphology and oocyte cytoplasm streaming, respectively). Time-lapse reconstitutions were made for each imaged egg chamber. Individual egg chamber growth and development was manually analyzed. The ratio between the nurse cell cluster and egg chamber lengths (NC/EC) was manually measured for all the points. Time zero ($T=0$) was defined as the first time point when NC/EC = 0.5. For each egg chamber, time measurements previous to $T=0$ are negative, whereas posterior measurements are positive. Individual measurements were collected, and average ± standard error was calculated. Slow ($T<0$) and fast ($T>0$) cytoplasm transfer average rates were respectively calculated for the 60 min before and after $T=0$. Linear regressions were fitted for both slow and fast phase measurements, and average rates calculated as a function of the average step for each regression.

Image analysis and treatment

LAS AF Lite (Leica Microsystems CMS GmbH), Fiji (NIH), and Photoshop (Adobe Systems) were used for image analysis and treatment.

Statistical analysis

Microsoft Office Excel™ (Microsoft 2012) and Prism 5.00 for Windows (GraphPad Software, San Diego, CA, USA) were used for graphical representation and statistical analysis.

Results

Abnormal nurse cell dumping in pkn mutant egg chambers

The ability to generate mutant mosaics of a zygotic lethal mutation allows the phenotypic analysis of genetically distinct groups of cells that otherwise could not be assessed (St Johnston, 2002). The FLP/FRT system is routinely used in *Drosophila* to induce mitotic recombination and generate mutant clones in a heterozygote organism. The FLP/FRT Ovo^{D} system eliminates non-recombinant female germ cells during early oogenesis (Chou and Perrimon, 1992); being the only viable egg chambers the ones that lost in the germ line the dominant mutation Ovo^{D}. This allows the generation of germ line clones, where all mid/late oogenesis egg chambers and laid eggs are

Fig. 1. Abnormal nurse cell dumping in *pkn* mutant egg chambers. (A) Normal egg laying in females whose germ line was mutant for Complementation Group 8 alleles (CG8: A5-88 and C58-31) (two-way anova, $p=0.5428$). No significant differences were observed both in the total number of eggs and egg laying distribution between CG8 mutant alleles and control females (two-way anova, $p>0.05$, for all genotype combinations and at any given time point). FRT42B was used as control for mitotic recombination. (B) Egg length was reduced in both mutant alleles of CG8. Average egg lengths were calculated: wild-type (Oregon R) = 626.3 ± 31.32 μm (average ± standard deviation, $n=191$), FRT42B = 608.4 ± 43.94 μm (control for the mitotic recombination, $n=148$), FRT42B *san* = 629.9 ± 48.43 μm (a non-related mutant allele isolated in the same screen that was used as a genetic background control, $n=100$ (Pimenta-Marques et al., 2008)), FRT42B A5-44 = 542 ± 89.94 μm ($n=155$), and FRT42B C58-31 = 511.5 ± 99.24 μm ($n=156$). Eggs mutant for both alleles of CG8 were significant shorter than all three controls used (one-way anova, $p<0.0001^{***}$). Both CG8 mutant alleles were not significantly different from each other (one-way anova, $p>0.05$). (C–F) Eggs mutant for both alleles of CG8 were significant shorter, yet dorsal appendages were in most cases normally positioned. (G′) Both mutant alleles of CG8 contained point mutations within *pkn* open-reading frame: A5-44, hereafter named *pkn*^{1T}, contained a splice site point mutation within the kinase domain of *pkn* (V1278, CTG/A). This potentially caused intron retention and mistranslation of the intronic fragment after residue position 1277. C58-31, hereafter named *pkn*^{2T}, contained a nonsense point mutation within the regulatory binding domain (RBD) of *Pkn*, from a glutamate (G) into a stop codon at the position 177 (TAC/T). This potentially resulted in a severely truncated protein. (G″) Western-blot analysis for embryonic total protein extracts using a polyclonal anti-Pkn antibody. Pkn protein levels were dramatically reduced in both isolated *pkn* mutant alleles (maternal mutants). The predicated sizes of Pkn protein isoforms vary from 129.5 kDa (Pkn-PO) to 163.9 kDa (Pkn-PN) (Flybase). A similar reduction was also observed in embryos mutant for *pkn*^{06736}, a previously reported mutant allele of *pkn* (Lu and Settleman, 1999). (H) Eggs mutant for the isolated *pkn* mutant alleles (*pkn*^{1T} and *pkn*^{2T}) and the previously isolated *pkn*^{06736} were equally short (*pkn*^{06736} = 570.9 ± 63.73 μm ($n=132$) (one-way anova, $p>0.05$), but all were significantly different from the control (one-way anova, $p<0.001$, ***). Control, *pkn*^{1T}, and *pkn*^{2T} results are the same as the ones shown in panel B. (I) The membrane between the nurse cell cluster and the oocyte (nurse cell-to-oocyte barrier) is continuous in control egg-chambers (FRT42B). (J–L) *pkn* mutant egg chambers showed a collapse of the nurse cell-to-oocyte barrier. (M) Quantification of the collapse of the nurse cell-to-oocyte membrane in stage 10 egg-chambers: Control (FRT42B) = 5% ($n=41$), FRT42B *pkn*^{1T} = 55% ($n=26$), and FRT42B *pkn*^{2T} = 58% ($n=30$). The FLP/FRT system was used to generate germ line mutant egg chambers. (I–K) Images are single confocal sections, whereas (L) is a Z-maximum projection. (I–K) Ovaries were stained for DNA (green) and F-actin (red). (L) Ovaries were stained for WGA (green) and F-actin (red). Scale bars: 100 μm (C–F) and 50 μm (I). Stage 10B egg chambers (I–L).

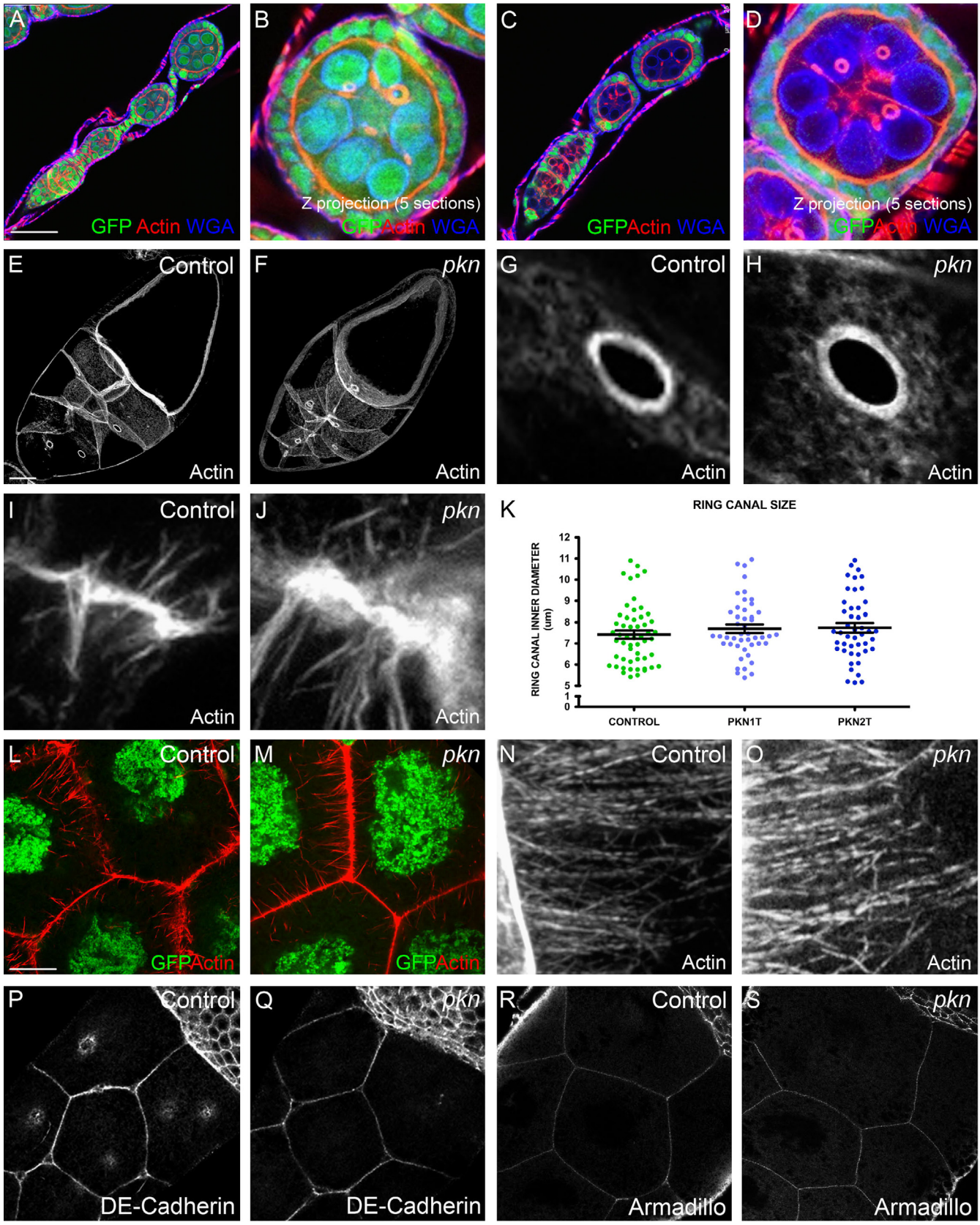

Fig. 2. Early and mid-oogenesis are essentially normal in *pkn* mutant egg chambers. (A–D) Early oogenesis in control (positive for nlsGFP) and *pkn* mutant germ line clones (negatively marked for nlsGFP) was normal, without detectable division defects of the germ line stem cells and cystoblasts. Both control and *pkn* mutant egg chambers contained the expected number of cells (15 nurse cells + 1 oocyte) and ring canals (15 ring canals) [Number of egg chambers: n(FRT42B) = 15 egg-chambers, n(FRT42B pkn^{1T}) = 20, n(FRT42B pkn^{2T}) = 19]. (E, F) Oocyte determination and growth during early and mid-oogenesis was normal in *pkn* mutant germ line clones. Ring canals in control and *pkn* mutant egg chambers were identical, with normal polymerization of F-actin (I, J) and a similar inner diameter (G, H; Quantification in K). Control (FRT42B) ring canal inner diameter was 7.437 ± 1.482 μm (average size ± standard deviation, n = 54), in FRT42B pkn^{1T} was 7.763 ± 1.429 μm (n = 46), and in FRT42B pkn^{2T} was 7.735 ± 1.476 μm (n = 45). No statistical differences were observed between both mutant alleles and the control (one-way anova, $p > 0.05$ in all). (L–O) Cytoplasmic actin filaments in control and *pkn* mutant egg chambers were identical. (P–S) DE-Cadherin and Armadillo localized correctly to the nurse cells *adherens junctions* of *pkn* mutant egg chambers. The FLP/FRT system was used to generate germ line mutant egg chambers. (A, C, G, H, L–S) Images are single confocal sections, whereas all the remaining images are Z-maximum projections. Ovaries were stained for nlsGFP (green), F-actin (red) and WGA (blue) in (A–D), were stained for F-actin (grey) in (E–J, N, O), were stained for DNA (green) and F-actin (red) in (L, M), were stained for DE-Cadherin (grey) in (P, Q), and were stained for Armadillo (grey) in (R, S). Scale bars: 50 μm (A), 50 μm (E), and 100 μm (L). Stage 10A egg chambers (E–H). Stage 10B egg chambers (I–S).

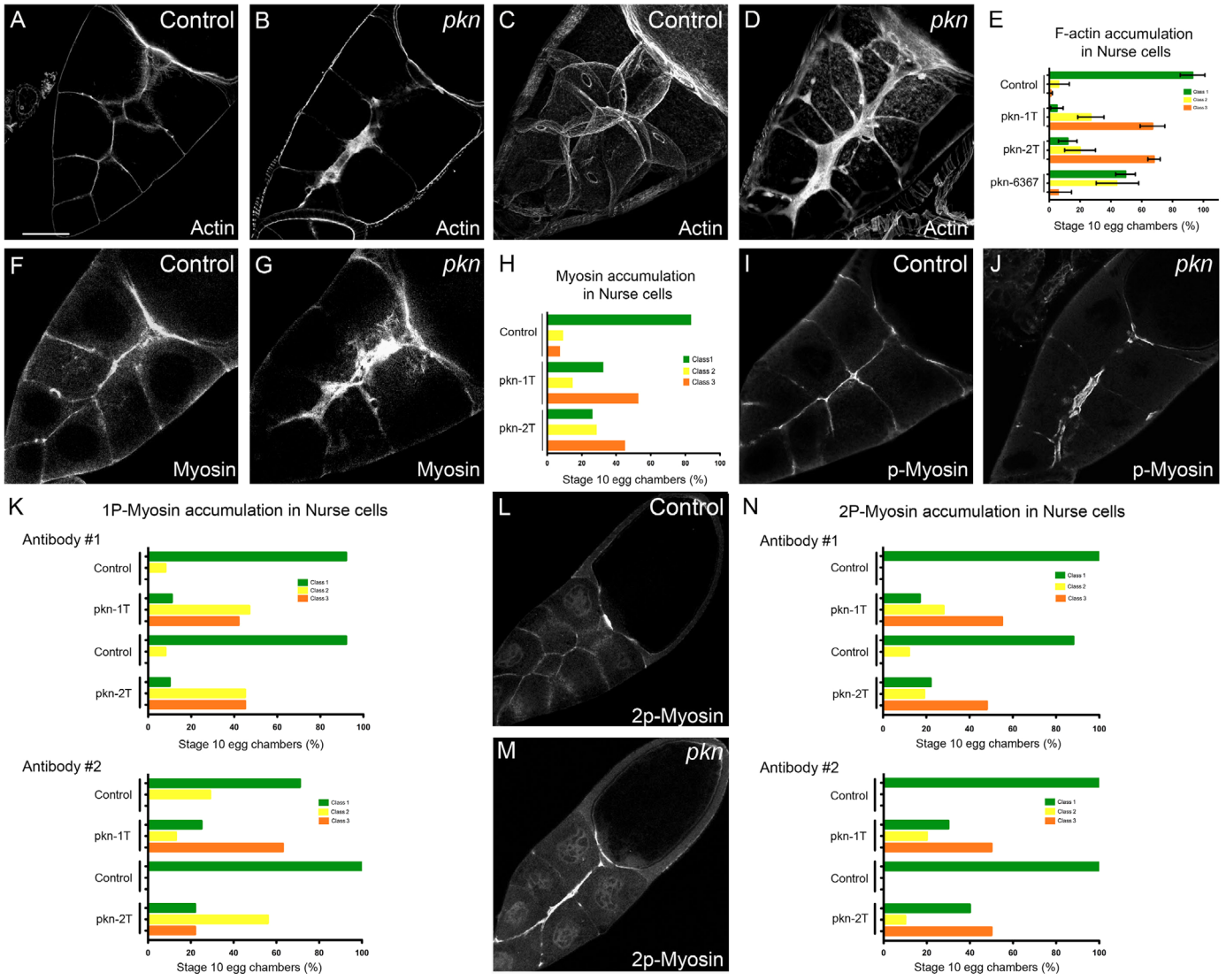

Fig. 3. *Pkn* is a negative regulator of actin–myosin activity during nurse cells dumping. (A–D) Abnormal accumulation of cortical F-actin in nurse cells mutant for *pkn* (stage 10B egg chambers). (E) Quantification of F-actin accumulation using three scoring classes: class 1-low cortical F-actin accumulation, class 2-intermediate accumulation, and class 3-high accumulation. Percentage of egg chambers that belong to each class: control (FRT42B): class 1=93 ± 8% (average ± standard deviation), class 2=6 ± 7%, class 3=1 ± 1% (n=94); FRT42B pkn^{1T}: class 1=5 ± 4%, class 2=27 ± 9%, class 3=67 ± 8% (n=75); FRT42B pkn^{2T}: class 1=12 ± 6%, class 2=20 ± 10%, class 3=68 ± 4% (n=42); FRT42B pkn^{06736}: class 1=50 ± 6%, class 2=44 ± 14%, class 3=6 ± 8% (n=14). (F, G) Abnormal accumulation of cortical Myosin II regulatory light chain subunit (Sqh-GFP) in nurse cells mutant for *pkn* (stage 10B egg chambers). (H) Quantification of Sqh-GFP accumulation using three scoring classes (as done for F-actin accumulation). Percentage of egg chambers that belong to each class: control (FRT42B): class 1=83.4%, class 2=9.2%, class 3=7.4% (n=54); FRT42B pkn^{1T}: class 1=32.4%, class 2=14.7%, class 3=52.9% (n=34); FRT42B pkn^{2T}: class 1=26.2%, class 2=28.6%, class 3=45.2% (n=42). (I, J) Abnormal accumulation of monophosphorylated Myosin II regulatory light chain (1P-Myosin) in nurse cells mutant for *pkn* (stage 10B egg chambers) (antibody #2; (Zhang and Ward, 2011)). (K) Quantification of 1P-Myosin accumulation (p-Ser21) using two different phosphospecific antibodies: antibody #1=Cell Signaling (#3671) and antibody #2 was a gift from Dr. Robert Ward (Zhang and Ward, 2011), and three scoring classes (as done for F-actin accumulation). Percentage of egg chambers that belong to each class: control (FRT42B) (antibody #1): class 1=92%, class 2=8%, class 3=0% (n=26); control (FRT42B) (antibody #2): class 1=86%, class 2=15%, class 3=0% (n=12); FRT42B pkn^{1T} (antibody #1): class 1=11%, class 2=47%, class 3=42% (n=26); FRT42B pkn^{1T} (antibody #2): class 1=25%, class 2=13%, class 3=63% (n=8); FRT42B pkn^{2T} (antibody #1): class 1=10%, class 2=45%, class 3=45% (n=11); FRT42B pkn^{2T} (antibody #2): class 1=22%, class 2=56%, class 3=22% (n=9). (L, M) Abnormal accumulation of dual phosphorylated Myosin II regulatory light chain (2P-myosin) in nurse cells mutant for *pkn* (stage 10B egg chambers) (antibody #2; (Zhang and Ward, 2011)). (N) Quantification of 2P-Myosin (p-Thr20 p-Ser21) accumulation using two different phosphospecific antibodies: antibody #1=cell signaling (#3674) and antibody #2 was a gift from Dr. Robert Ward (Zhang and Ward, 2011), and three scoring classes (as done for F-actin accumulation). Percentage of egg chambers that belong to each class: control (FRT42B) (antibody #1): class 1=94%, class 2=6%, class 3=0% (n=41); control (FRT42B) (antibody #2): class 1=100%, class 2=0%, class 3=0% (n=19); FRT42B pkn^{1T} (antibody #1): class 1=17%, class 2=28%, class 3=55% (n=29); FRT42B pkn^{1T} (antibody #2): class 1=30%, class 2=20%, class 3=50% (n=10); FRT42B pkn^{2T} (antibody #1): class 1=22%, class 2=19%, class 3=48% (n=21); FRT42B pkn^{2T} (antibody #2): class 1=40%, class 2=10%, class 3=50% (n=10). All images are single confocal sections, except (C, D) that are Z-maximum projections of confocal sections. The FLP/FRT system was used to generate the germ line mutant egg chambers. (A) Scale bar: 50 μm. Stage 10B egg chambers (all panels).

necessarily mutant for the gene of interest. Similarly, using a fluorescent reporter, germ line mutant egg chambers can be identified during oogenesis by the absence of nuclear GFP.

Complementation group 8 (CG8) includes two distinct mutant alleles (A5-44 and C58-31) (Pimenta-Marques et al., 2008). Female germ line clones of CG8 were generated using the FLP/FRT Ovo^{D} system (Chou and Perrimon, 1992). Egg laying was comparable to control (two-way anova, p=0.5428) (Fig. 1A), without any difference in either the number of eggs or distribution and the duration of egg laying peak between CG8 alleles and controls (two-way anova, $p > 0.05$, for all genotype combinations at any given time point) (Fig. 1A). Eggs laid by germ line CG8 mutant females were

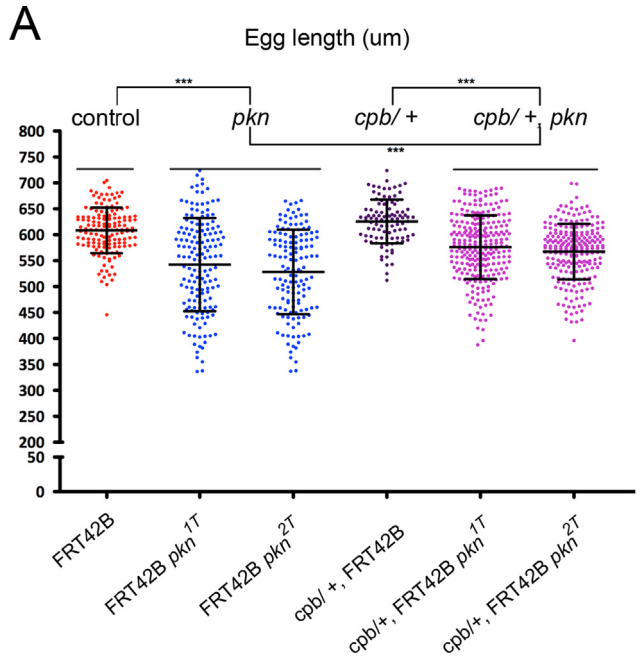

Fig. 4. A mutant recessive allele of *capping protein beta* is a dominant suppressor of *pkn*. (A) The strong hypomorphic allele of *capping protein beta* (cpb^{M143}), dominantly suppressed the short-egg phenotype of both *pkn* mutant alleles: control (FRT42B)=629.9 ± 48.43 μm (average ± standard deviation, n=148); FRT42B pkn^{1T}=542 ± 89.94 μm (n=155); FRT42B pkn^{2T}=511.5 ± 99.24 μm (n=156), cpb^{M143}/+, FRT42B=625.6 ± 42.05 μm (n=101); cpb^{M143}/+, FRT42B pkn^{1T}= 576.0 ± 61.41 μm (n=266); cpb^{M143}/+, FRT42B pkn^{2T}=567.5 ± 53.52 μm (n=229). The dominant suppression by cpb^{M143} was statistically significant (one-way anova, $p<0.001$, ***) for all genotypes. Control, pkn^{1T}, and pkn^{2T} results shown in this figure are the same as the ones shown in Fig. 1B.

on average significantly shorter than controls (Fig. 1B–F) (one-way anova, $p<0.0001$), with dorsal appendages usually normally positioned (Fig. 1C–F). This suggested that, although the eggs were short, dorsal–ventral (DV) patterning of mutant eggs was mostly unaffected.

The 2R Deficiency kit (Bloomington stock collection) was used to map both CG8 alleles to cytological interval 45A6-A9 (see methods for detail; data not shown). By candidate gene approach we concluded that both CG8 alleles failed to complement the zygotic lethality of six known lethal P-elements of *pkn*: pkn^{3} (BL5523), pkn^{2} (BL6103), pkn^{K11209} (BL11018), pkn^{RG232} (BL12052), $pkn^{KG02139}$ (BL14584) and pkn^{06736} (BL12322). pkn^{06736} has been previously published as a strong hypomorphic allele of *pkn* (Lu and Settleman, 1999). Genomic DNA sequencing of both CG8 alleles identified distinct point mutations within the *pkn* open-reading frame (Fig. 1G′). The A5-44 allele, hereafter named pkn^{1T}, contained a splice site mutation within the kinase domain of *pkn* (V1278, CTG/A). This is predicted to cause intron retention, mistranslation of the intronic fragment after the amino acid at position 1277, and truncation of Pkn kinase domain. Allele C58-31, hereafter named pkn^{2T}, contained a nonsense point mutation within the regulatory binding domain (RBD) of Pkn, from a glutamate (G) into a stop codon at the position 177 (TAC/T). This is predicted to result in a severely truncated protein. Both pkn^{1T} and pkn^{2T} maternal mutant embryos showed great reduction in Pkn protein levels (Fig. 1G″). A similar reduction was also obtained with a previously published *pkn* p-element insertion mutant, pkn^{06736} (Fig. 1G″) (Lu and Settleman, 1999). Female germ line clones of pkn^{06736} phenocopied the short-egg phenotypes of pkn^{1T} and pkn^{2T} alleles (Fig. 1H). Germ line mutant FRT42B pkn^{06736} females laid eggs that were significantly smaller than controls (one-way anova, $p<0.0001$), but not significantly different than pkn^{1T} and pkn^{2T} mutant alleles (one-way anova, $p>0.05$) (Fig. 1H).

Nurse cell dumping is the process by which the fifteen nurse cells of an egg chamber, contract and transfer their cytoplasmic content through the ring canals into the growing oocyte (Wheatley et al., 1995). During dumping, egg chambers mutant for *pkn* frequently showed a collapse of the membrane that separates nurse cell cluster from oocyte (Fig. 1I–L), leading to the abnormal presence of either ring canals, border cells and/or nurse cell nuclei in the oocyte cytoplasm (Fig. 1I–L, asterisk in J and L). In control egg chambers, only 5% of egg chambers showed a nurse cell-to-oocyte membrane collapse (n=41). This increased to more than 50% in *pkn* mutant egg chambers [percentages of egg chambers with nurse cell-to-oocyte membrane collapse: pkn^{1T}=55% (n=26), pkn^{2T}=58% (n=30)] (Fig. 1M). Egg chambers mutant for a previously isolated allele of *pkn* (pkn^{06736}) also showed nurse cell-to-oocyte membrane collapse (Fig. 1K). The nurse-cell-to-oocyte membrane collapse was also observed after immunostainings with DE-Cadherin, Armadillo, and atypical protein kinase C (aPKC) (data not shown). Our results demonstrate that Pkn is required within the germ line for egg chamber integrity and normal nurse cell dumping during oogenesis.

Early and mid-oogenesis are essentially normal in pkn mutant egg chambers

Drosophila females whose germ line was mutant for *pkn* showed normal egg laying. *pkn* mutant germ line clones (negatively marked for GFP) developed normally during early oogenesis without any detectable phenotype (Fig. 2A–D). Both control and *pkn* mutant egg chambers contained the expected number of cells (15 nurse cells+1 oocyte) and ring canals (15 ring canals) [Number of egg chambers: n(FRT42B)=15 egg-chambers, n (FRT42B pkn^{1T})=20, n(FRT42B pkn^{2T})=19]. Mid-oogenesis was also mostly normal in *pkn* mutant egg chambers, although in this case there was a detectable subset of nurse cells whose nurse cell-to-nurse cell membrane collapsed within an otherwise normal egg chamber. In controls, 3.3% ± 1.0 of egg chambers showed nurse cell-to-nurse cell membrane collapse (average ± standard deviation) (n=61); whilst in *pkn* mutant egg chambers there was an increase of the frequency of such phenotype [pkn^{1T} (20.7% ± 1.0, n=29) and in pkn^{2T} (19.4% ± 2.1, n=31)]. The multinucleated nurse cells phenotype was only observed after stage 6/7 egg chambers. This suggested that although cytokinesis was normal in the germarium, a weakness in the nurse cells membrane was likely to exist. Since in human cells PRK2 is important for cell adhesion and apical junctions maturation (Calautti et al., 2002; Wallace et al., 2011), we decided to investigate if *Drosophila* Pkn was required for assembly and/or maturation of nurse cell *adherens junctions* (AJs). We failed to detect any consistent change in the expression of distinct junctional proteins in egg chambers mutant for *pkn* (Fig. 2P–S) (data not shown). Consistently, somatic follicular epithelial cells mutant for *pkn* also showed normal epithelial architecture during early oogenesis (Supplementary Fig. 7)(data not shown). Embryonic dorsal closure defects observed in zygotic mutant for *pkn* also occurred without apparent loss of ectoderm integrity (Lu and Settleman, 1999).

Defects in the nurse cell ring canals and cytoplasmic actin filaments can potentially explain the dumping defects observed in egg chambers mutant for *pkn*. We did not detect any morphological (Fig. 2E–J) or size defects (Fig. 2K) (one-way anova, $p>0.05$ in all cases) of ring canals from *pkn* mutant egg chambers. The nurse cell cytoplasmic actin cables were also morphologically normal in most *pkn* mutant egg chambers (Fig. 2L–O). Our results

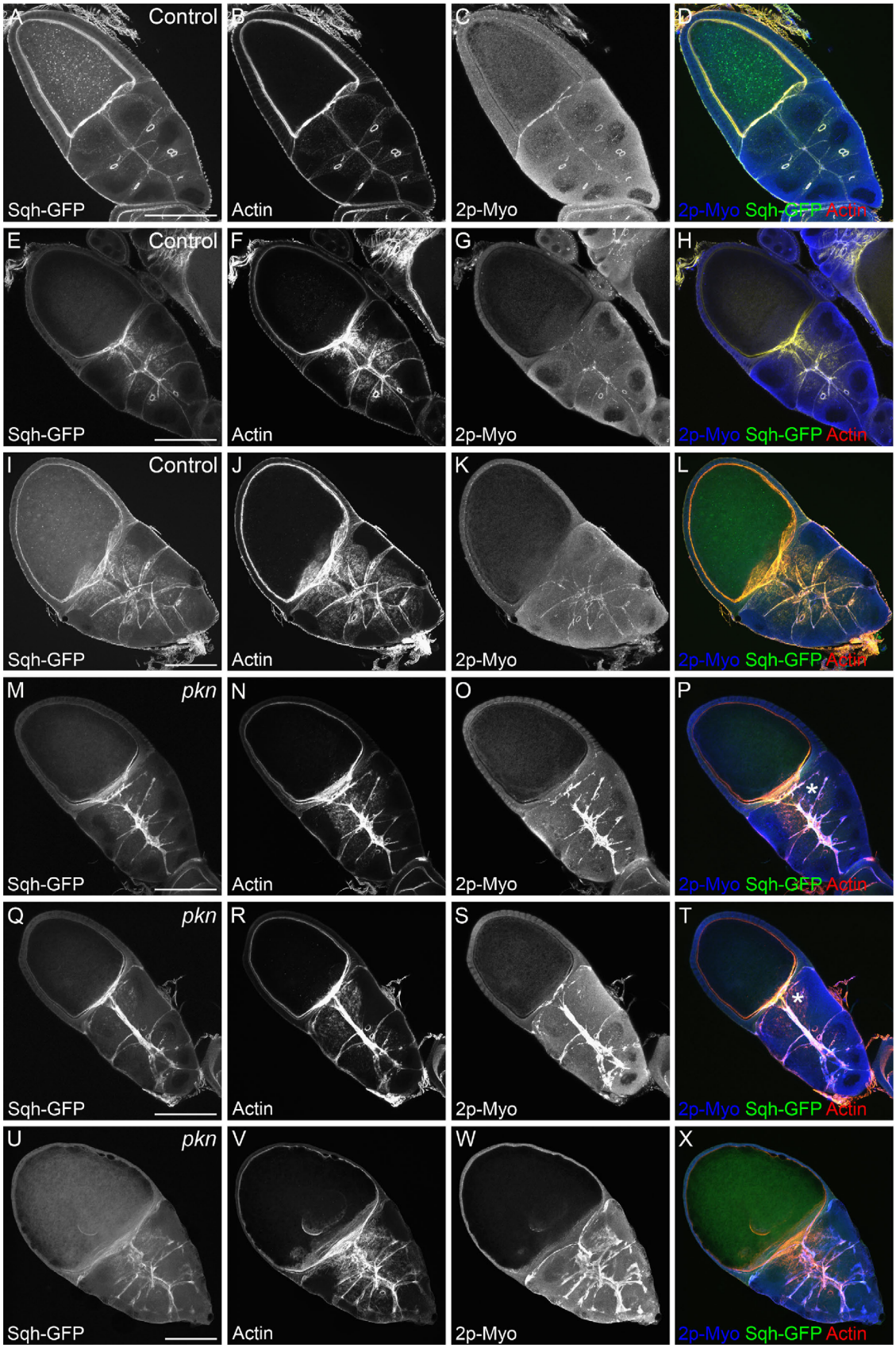

Fig. 5. *Pkn* spatially regulates nurse cells actin–myosin activity during dumping. (A–L) Wild type egg chambers had detectable levels of activated actin–myosin cytoskeleton (2P-myosin) in the cortical region of the nurse cells during fast dumping. (M–X) Nurse cells mutant for *pkn* showed not only a dramatic increase in the levels of activated actin–myosin (2P-myosin), but its morphology and spatial organization was highly abnormal (P, T, X): with excessive thickness (T), significant discontinuities that were suggestive of breakage (see asterisks in P and T), and a cytoskeleton that frequently radiated outwardly perpendicularly to the anterior-posterior axis of the egg chamber (X). All images are Z-maximum projections of confocal sections. The FLP/FRT system was used to generate the germ line mutant egg chambers. All ovaries were stained for Sqh-GFP (grey or green), F-actin (grey or red) and 2P-myosin (grey or blue). (A) Scale bar: 80 μm. Stage 10A egg chambers (A–D). Stage 10B egg chambers (E–X).

demonstrate that Pkn is not rate limiting during early oogenesis. They also suggest that at least in most cases, the nurse cell dumping defects observed in *pkn* mutant egg chambers are not due to cell-cell adhesion nor cytokinesis defects, neither are they due to abnormalities in nurse cell ring canals or cytoplasmic actin cables.

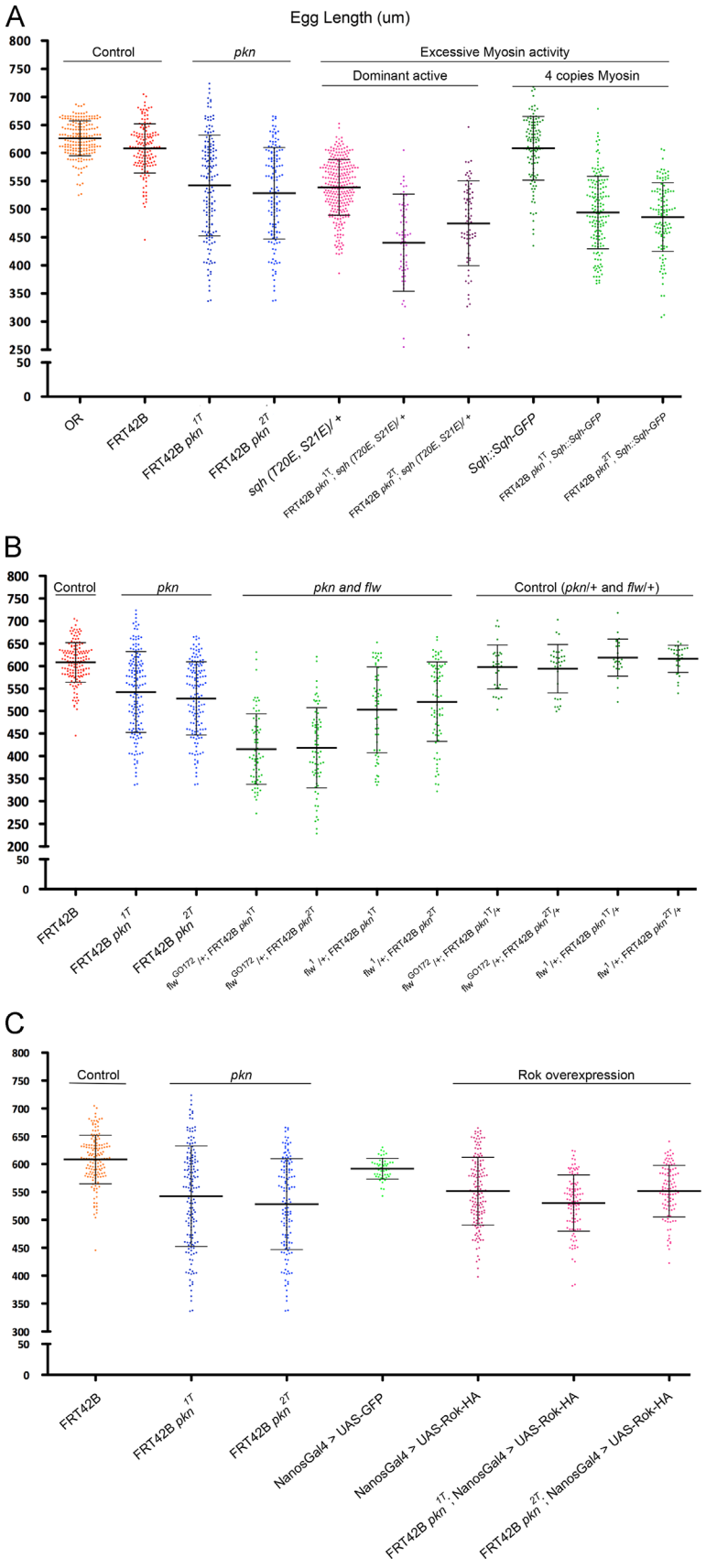

Abnormal accumulation of cortical F-actin in pkn mutant egg chambers

Nurse cell dumping is an actin–myosin based process. Although the actin cytoskeleton was apparently normal during early/mid-oogenesis, *pkn* mutant stage 10 egg chambers showed a dramatic accumulation of cortical F-actin in the nurse cell cluster just before the onset of fast dumping during stage 10B (Fig. 3A–D; quantification in 3E, class 1 = low accumulation levels of cortical F-actin, class 2 = intermediate accumulation, and class 3 = high accumulation; see methods for more detail and Supplementary Fig. 6). F-actin cortical enrichment occurred not only in the central region of the mutant nurse cell cluster, but also radiated out in a way consistent with the nurse cells membrane outline (Fig. 3C and D). The abnormal accumulation of cortical F-actin also occurred in *pkn* mutant egg chambers whose AJs junctional components were normal (Supplementary Fig. 1). We failed to detect any correlation between border cell migration defects and accumulation of F-actin in nurse cells mutant for *pkn* (data not shown).

Capping proteins alpha and beta (Cpa and Cpb) subunits form a functional heterodimer capable of regulating F-actin polymerization (Cooper and Sept, 2008). Egg chambers mutant for *cpb* have dumping defects and produce short-eggs (Gates et al., 2009), with phenotypes similar to the ones observed in *pkn* mutants. A strong hypomorphic allele of *cpb* (cpb^{M143}) was a dominant suppressor of the *pkn* mutant short-egg phenotype (Fig. 4A) (one-way anova, $p < 0.001$). cpb^{M143} was also a dominant suppressor of nurse cell cluster F-actin accumulation (Supplementary Fig. 2A and B; quantification in 2C). Our results show that Pkn negatively regulates F-actin accumulation in the nurse cell cluster. The abnormal organization of the actin cytoskeleton is likely to be functionally relevant for the observed dumping and short-egg phenotypes of *pkn* mutants. It is also possible that Pkn is important for integrity of nurse cells cortical actin cytoskeleton, which becomes particularly rate limiting for tissue integrity during dumping. We hypothesize that F-actin mostly accumulates in the central region of the mutant egg chambers due to unknown signaling mechanisms that spatially regulate actin–myosin contractility during dumping.

Abnormal activation of actin–myosin cytoskeleton in pkn mutant egg chambers

In *Drosophila*, MRLC is encoded by *spaghetti squash* (*sqh*). Sqh is activated primarily by Serine 21 phosphorylation (1p-myosin; pSer21), and secondarily by phosphorylation of threonine 20 (2p-myosin; pSer21 and pThr20) (Ikebe et al., 1988; Zhang and Ward, 2011). Similar to F-actin, the levels of cortical myosin (SQH::sqh-GFP) were significantly increased in stage 10 *pkn* mutant nurse cells (Fig. 3F and G; Quantification in 3H). Since enriched myosin colocalized with cortical F-actin (Fig. 5A, B, M, and N), we hypothesized that Pkn was a negative regulator of actin–myosin cytoskeleton contractility during dumping. Stage 10 nurse cells mutant for *pkn* showed a significant increase in the levels of monophosphorylated (1p-myosin; pSer21) (Fig. 3I and J; quantification in 3K) and diphosphorylated (2p-myosin; pThr20 and pSer21) cortical myosin (Fig. 3L and M; quantification in 3N).

MRLC phosphorylation correlates with increased levels of actin–myosin cytoskeleton contractility (Jung et al., 2008). Wild type egg chambers showed detectable levels of activated myosin (2p-myosin) in the nurse cell cortex during dumping (Fig. 5A–L). *pkn* mutant egg chambers presented not only a dramatic increase in the levels of activated myosin, but also the morphology and localization of the activated actin–myosin cytoskeleton was highly abnormal (Fig. 5M–X). In *pkn* mutant egg chambers the activated actin–myosin cytoskeleton was abnormally thick in the nurse cell cluster (Fig. 5P and T), showed significant discontinuities (Fig. 5P and T; see asterisks), and radiated outwardly perpendicular to the anterior–posterior axis of the egg chamber (Fig. 5X). Our results show that Pkn negatively regulates actin–myosin activation (and most likely contractility) during nurse cell dumping.

Nurse cell dumping defects of pkn mutant egg chambers are due to excessive actin–myosin activation

Actin–myosin cytoskeleton contractility is regulated by the equilibrium between distinct kinases (e.g., MLCK, ROK, ZIP) and phosphatases (in most cases, Myosin phosphatase, PP1) activities (Grassie et al., 2011; Matsumura, 2005). Egg chambers whose germ line was mutant for *pkn* showed abnormally high levels of actin–myosin phosphorylation in the nurse cells. If the short-egg phenotypes resulted from excessive activation of the nurse cells actin–myosin cytoskeleton, then an increase in the levels of myosin activity was likely to enhance and/or recapitulate *pkn* phenotypes. If Pkn behaved as a negative regulator of MRLC activation than an increase in the total levels of MRLC was likely to exacerbate the phenotypes observed in *pkn* mutants. Although doubling the total amount of MRLC (4× Sqh: 2× endogenous Sqh + 2× Sqh-GFP) did not affect egg lengths (Fig. 6A), in a *pkn* mutant background, it further reduced the average size of the eggs (Fig. 6A) (one-way anova, $p < 0.001$).

If the phenotypes observed in *pkn* mutant egg chambers resulted from an abnormal phosphorylation of MRLC than a

Fig. 6. *Pkn* mutant short-egg phenotype is phenocopied and dominantly enhanced by increased levels of actin–myosin activity. All graphs show individual egg lengths (μm) (*Y*-axis). Genotypes are indicated in the graph *X*-axis. (A) Activated myosin, $sqh^{T20E,S21E}/+$ not only phenocopied the short-egg phenotype of *pkn* mutants, but dominantly enhanced *pkn* in the presence of a wild-type copy of Sqh. Increasing the total protein levels of myosin (Sqh) using a Sqh-GFP construct under the control of an endogenous promoter (4 copies of Sqh: 2 copies Sqh::GFP plus the two endogenous copies) enhanced both *pkn* mutant alleles. Control (FRT42B) = 629.9 ± 48.43 μm (average size ± standard deviation, $n = 148$); FRT42B pkn^{1T} = 542 ± 89.94 μm ($n = 155$); FRT42B pkn^{2T} = 511.5 ± 99.24 μm ($n = 156$); $sqh^{T20E,S21E}/+$ = 538.8 ± 49.40 μm ($n = 281$); FRT42B pkn^{1T}; $sqh^{T20E,S21E}/+$ = 440.4 ± 86.49 μm ($n = 70$); FRT42B pkn^{2T}; $sqh^{T20E,S21E}/+$ = 474.9 ± 75.44 μm ($n = 73$); sqh::SQH-GFP = 608.6 ± 57.06 μm ($n = 115$); FRT42B pkn^{1T}, sqh::SQH-GFP = 494.0 ± 64.43 μm ($n = 153$); FRT42B pkn^{2T}, sqh::SQH-GFP = 486 ± 61.08 μm ($n = 116$). FRT42B *pkn*, sqh::SQH-GFP and FRT42B *pkn*; sqhT20E,S21E/+ were significantly different from FRT42B *pkn* (one-way anova, $p < 0.001$ in all cases). (B) A strong mutant allele (flw^{GO172}) for the catalytic subunit of myosin phosphatase 1 (Flw, flapwing), whose phosphatase activity inhibits actin–myosin activity, was a dominant enhancer of *pkn*. This enhancement occurred according to the allelic series of the *flw* mutant alleles used: flw^{1} is a weak hypomorphic allele (no enhancement), whereas flw^{GO172} is a strong hypomorphic allele (significant enhancement). Control (FRT42B) = 629.9 ± 48.43 μm (average size ± standard deviation, $n = 148$); FRT42B pkn^{1T} = 542 ± 89.94 μm ($n = 155$); FRT42B pkn^{2T} = 511.5 ± 99.24 μm ($n = 156$); $flw^{1}/+$; FRT42B pkn^{1T} = 503.0 ± 95.54 μm ($n = 56$); $flw^{1}/+$; FRT42B pkn^{2T} = 521.0 ± 88.55 μm ($n = 79$); $flw^{1}/+$; FRT42B $pkn^{1T}/+$ = 619.0 ± 41.14 μm ($n = 24$); $flw^{1}/+$; FRT42B $pkn^{2T}/+$ = 616.4 ± 29.97 μm ($n = 28$); $flw^{GO172}/+$; FRT42B pkn^{1T} = 415.5 ± 78.26 μm ($n = 69$); $flw^{GO172}/+$; FRT42B pkn^{2T} = 418.6 ± 88.96 μm ($n = 72$); $flw^{GO172}/+$; FRT42B $pkn^{1T}/+$ = 598.2 ± 48.80 μm ($n = 32$); $flw^{GO172}/+$; FRT42B $pkn^{2T}/+$ = 594.4 ± 53.69 μm ($n = 32$). $flw^{1}/+$; FRT42B *pkn* were not significantly different from FRT42B *pkn* (one-way anova, $p > 0.05$). Yet, both were significantly from the respective controls (one-way anova, $p < 0.001$). $flw^{GO172}/+$; FRT42B *pkn* were significantly different from FRT42B *pkn* (one-way anova, $p < 0.001$). (C) Overexpression of Rho-dependent kinase (ROK), a positive regulator of actin–myosin activity, phenocopied *pkn* short-egg phenotype, but it did not enhance *pkn*. Control (FRT42B) = 629.9 ± 48.43 μm (average size ± standard deviation, $n = 148$); FRT42B pkn^{1T} = 542 ± 89.94 μm ($n = 155$); FRT42B pkn^{2T} = 511.5 ± 99.24 μm ($n = 156$); NanosGAL4 > UAS::GFP = 591.7 ± 18.65 μm ($n = 49$); NanosGAL4 > UAS::HA-ROK = 550.5 ± 60.58 μm ($n = 148$); FRT42B pkn^{1T}; NanosGAL4 > UAS::HA-ROK = 530.2 ± 50.41 μm ($n = 103$); FRT42B pkn^{2T}; NanosGAL4 > UAS::HA-ROK = 551.6 ± 46.09 μm ($n = 101$). NanosGAL4 > UAS::HA-ROK, FRT42B pkn^{1T}; NanosGAL4 > UAS::HA-ROK, and FRT42B pkn^{2T}; NanosGAL4 > UAS::HA-ROK were significantly different from controls (FRT42B and NanosGal4 > UAS::GFP) (one-way anova, $p < 0.001$ in all cases). They were however not significantly different from each other (one-way anova, $p > 0.05$, in all cases). Control, pkn^{1T}, and pkn^{2T} results shown in this figure are the same as the ones shown in Fig. 1B.

phospho-mimetic form of MRLC should phenocopy *pkn* mutant alleles. Furthermore, and in the presence of a wild-type copy of MRLC, *pkn* mutations should be able to further enhance the phenotypes observed with a phospho-mimetic form of MRLC. Expression of a phospho-mimetic form of MRLC (sqhT20E, S21E) known to behave as a dominant active myosin (Winter et al., 2001), not only recapitulated the short-egg phenotype of *pkn* mutants (Fig. 6A), but significantly enhanced (in the presence of a wild-type copy of MRLC) both *pkn* mutant alleles phenotypes (Fig. 6A) (one-way anova, $p<0.001$). Dominant active MRLC (sqhT20E, S21E) recapitulated not only the short-egg phenotype, but also the nurse cell-to-oocyte membrane collapse (Supplementary Fig. 3A and B; quantification in 3C), and nurse cell cluster accumulation of cortical F-actin (Supplementary Fig. 3D and E; quantification in 3F).

Rho-dependent kinase (Rok) is a positive regulator of actin–myosin contractility (Kimura et al., 1996; Leung et al., 1996). Over-expression of Rok (using a UAS-HA-ROK construct) was sufficient to recapitulate the *pkn* mutant short-egg phenotype (one-way anova, $p<0.001$) (Fig. 6C). In contrast to dominant active MRLC (SqhT20E, S21E), over-expression of Rok did not enhance the short-egg phenotype of *pkn* (one-way anova, $p>0.05$) (Fig. 6C). Although we still lack a mechanistic explanation, we concluded that Rok is most likely genetically downstream to Pkn. MRLC can be dephosphorylated, and consequently inactivated, by PP1 (protein phosphatase 1). DMBS (*Drosophila* myosin binding subunit) is the regulatory binding protein of PP1 (Mizuno et al., 2002). Removing one copy of DMBS did not modify the short-egg phenotype of *pkn* (data not shown). Flapwing (Flw) is the catalytic subunit of PP1 (Raghavan et al., 2000). flw^{1}, a weak hypomorphic allele of *flapwing*, did not behave as a dominant enhancer of *pkn* (one-way anova, $p>0.05$) (Fig. 6B). flw^{G0172}, a strong mutant allele, significantly enhanced the short-egg phenotype of *pkn* (one-way anova, $p<0.001$) (Fig. 6B). Our results demonstrated *pkn* dumping defects and short-egg phenotypes were phenocopied and/or enhanced by distinct mutant alleles known to increase MRLC phosphorylation. We concluded *pkn* phenotypes during oogenesis most likely resulted from an abnormal activation of the actin–myosin cytoskeleton within the nurse cells.

Pkn is required for an efficient transfer rate of the nurse cell cytoplasm into the growing oocyte

Egg chambers whose germ line was mutant for *pkn* showed nurse cell dumping defects, with frequent collapse of the nurse cell-to-oocyte barrier and the production of short-eggs. These phenotypes resulted most likely from abnormally high levels of actin–myosin phosphorylation within the nurse cells cluster. We hypothesized that nurse cell contractility must be temporally and spatially well coordinated for an efficient cytoplasmic transfer rate during dumping. To investigate if the cytoplasmic flow rate was abnormal in *pkn* mutant egg chambers we developed an *ex-vivo* nurse cell dumping assay based on previous reported protocols (Morris and Spradling, 2011; Prasad et al., 2007). Freshly dissected ovaries were incubated in culture medium, and egg chambers observed under a fluorescence microscope (see methods for more details). For live-cell imaging were only used egg chambers without any detectable nurse-cell-to-oocyte membrane collapse, normal cytoplasmic streaming and normal nuclear morphology at the beginning of data acquisition. Nurse cell dumping can be divided in a slow phase, when specific molecules are transported into the oocyte, and a fast phase, during which the nurse cells empty all their remaining cytoplasmic content into the growing oocyte (Mahajan-Miklos and Cooley, 1994).

Time zero was defined in all movies as the first moment when the total length of the nurse cell cluster (NC) is approximately 50% of the total length of the egg chamber (EC) (NC/EC=0.5) (Fig. 7A). Analysis of control egg chambers showed the average dumping rate [Δ (nurse cell cluster length (NC)/egg chamber length (EC))/time] to be significantly slower in younger egg chambers (NC/EC > 0.5) compared to older egg chambers (NC/EC < 0.5) (Fig. 8A and B, Supplementary Fig. 5A) (Movie 1; picture stills are shown in Fig. 7A). This is consistent with the expectation that the transition between slow and fast dumping occurs in stage 10B egg chambers when NC/EC becomes smaller than 0.5. During slow dumping (NC/EC > 0.5) the average dumping rates were not significantly different between control and *pkn* mutant egg chambers [control=0.05% per minute, $n=21$; pkn^{1T}=0.05% per minute, $n=18$; pkn^{2T}=0.06% per minute, $n=18$] (Fig.8A and B, Supplementary Fig. 5A), whereas during fast dumping (NC/EC < 0.5) average dumping rates were significantly faster (0–60 min after NC/EC=0.5) in control when compared to *pkn* mutant egg chambers [control=0.28% per minute, $n=21$; pkn^{1T}= 0.08% per minute, $n=18$; pkn^{2T}=0.17% per minute, $n=18$ ($p<0.0001$ for both cases)] (Fig. 7A–C, Fig. 8A and B, Supplementary Fig. 5A and B) (Movies 1 and 2; picture stills are shown in Fig. 7A and B). We concluded that the transition between slow and fast nurse cell dumping is a discrete event, with a dumping rate increase of at least five to six-fold. Defining time zero as NC/EC=0.5, although experimentally unbiased, does not account for biological variation for the onset of fast dumping during stage 10B (NC/EC < 0.5). This introduces a possible underestimation of the *in vivo* dumping rates and it is an explanation for the noticeable variation within individual wild-type egg chambers (green lines in Supplementary Fig. 4). Regardless, egg chambers mutant for *pkn* showed statistically significant dumping rate defects after NC/EC became smaller than 0.5 (fast dumping) (Supplementary Fig. 5A and B). We concluded that Pkn avoids excessive actin–myosin activity and helps to maintain nurse-cell-to-oocyte membrane integrity for efficient transfer of the nurse cells cytoplasm during fast dumping.

Supplementary material related to this article can be found online at http://dx.doi.org/10.1016/j.ydbio.2014.08.008.

Discussion

Nurse cell dumping is an actin–myosin based process where fifteen nurse cells of a given egg chamber contract and transfer their cytoplasmic content through the ring canals into the growing oocyte. In this work, we identified *Drosophila Pkn* as negative regulator of actin–myosin contractility. Egg chambers mutant for *pkn* showed significant nurse cell dumping defects and production of short-eggs. Several other regulators of actin–myosin contractility have previously been reported to be important for nurse cell dumping (e.g., Gates et al., 2009). Most of these mutants were invariably associated with multiple defects during female germ line development, while *pkn* mutant egg chambers showed no detectable defects in cytokinesis, cell adhesion and cell polarization during early oogenesis. Pkn was not required in the soma for establishment of follicle cells epithelial architecture (Supplementary Fig. 7), but its function was nevertheless important for somatic follicular morphogenesis during mid/late oogenesis (data not shown) and embryonic dorsal closure (zygotic mutants) (Lu and Settleman, 1999). Nurse cell dumping, somatic follicular morphogenesis, and embryonic dorsal closure involve highly coordinated tissue-wide contractility. We concluded that *Drosophila Pkn* is a negative regulator of actin–myosin activity, whose function is particularly rate limiting in a subset of morphogenetic processes that require highly coordinated contractile forces. Rok is a positive regulator of actin–myosin activity, whereas we observed that Pkn behaved as a negative regulator. Since Rho induces activation of Rok and Pkn kinases (Jung et al., 2008; Kimura et al., 1996; Leung et al., 1996; Lu and Settleman, 1999), we hypothesize that Pkn is

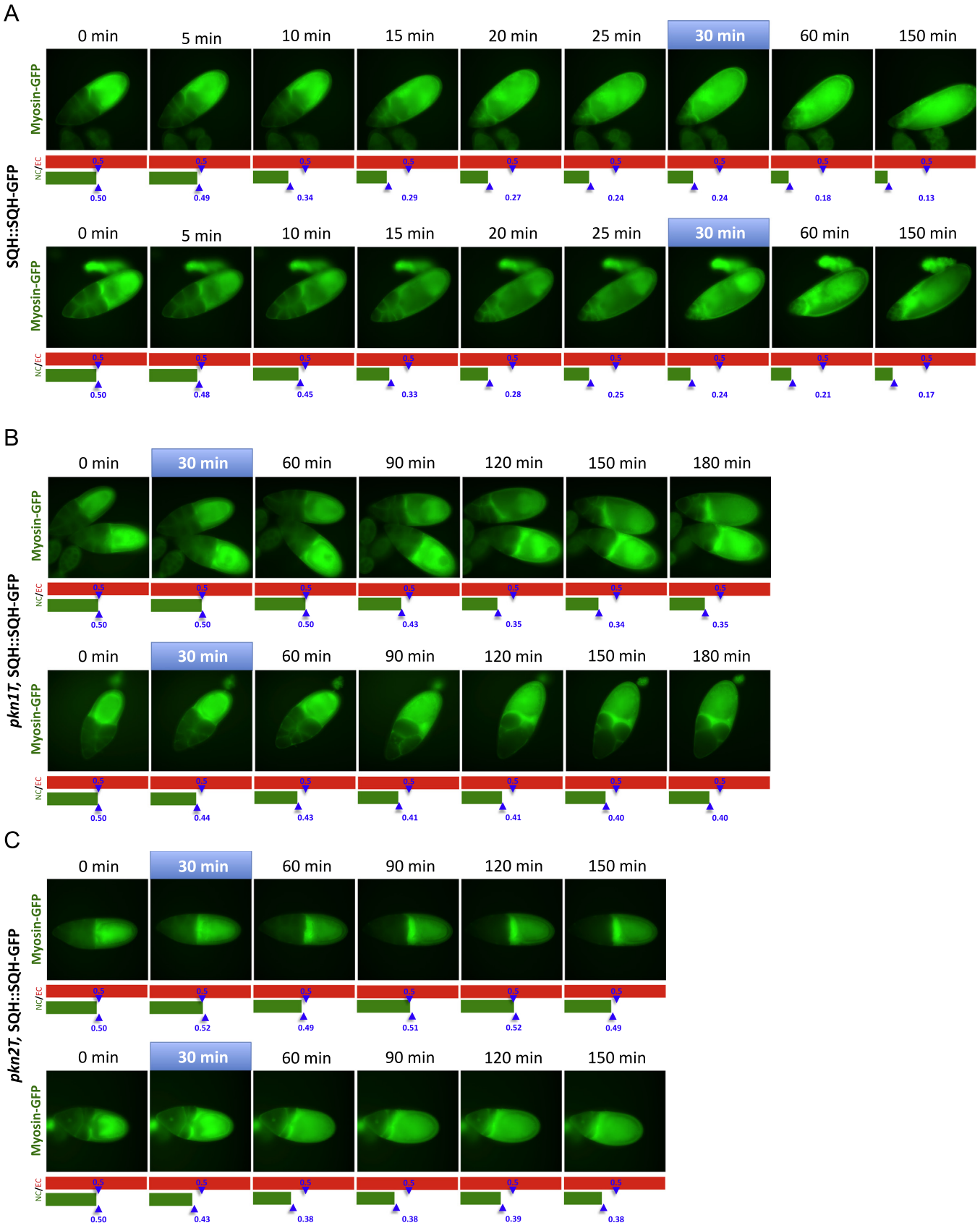

Fig. 7. Pkn is required for efficient nurse cell dumping. Selected time frames of *ex-vivo* nurse cell dumping movies. Freshly dissected ovaries were incubated with culture medium, and egg chambers were observed under a fluorescent microscope (see methods for more details). For live-cell imaging were only used egg chambers without any detectable nurse-cell-to-oocyte membrane collapse, normal cytoplasmic streaming and normal nuclear morphology at the beginning of data acquisition. Time zero was defined as the first moment when total length of the nurse cells cluster (NC)/total length of the egg chamber (EC) was equal to 0.5. (A) Sqh-GFP egg chambers (control) took approximately 30 min from NC/EC = 0.5 to reduce to 0.25. (B, C) Sqh-GFP egg chambers mutant for *pkn* (respectively: FRT42B pkn^{1T}, Sqh-GFP and FRT42B pkn^{2T}, Sqh-GFP) showed significantly slower fast dumping rates, as it took a significantly longer time after NC/EC = 0.5 for the egg chamber to reach NC/EC = 0.25. Egg chambers mutant for *pkn* frequently failed to reduce any further than 0.3 within the experiment time frame (Supplementary Fig. 4). Top panels show the myosin cytoskeleton (Spaghetti Squash-GFP) (green). Lower panels are graphic representations of the corresponding NC/EC ratios at the depicted time points. Blue triangles represent the initial NC/EC = 0.5 (top) and the NC/EC at the depicted time point (bottom). Red bars represent the total egg length and the green bars represent the length of the nurse cell cluster. Morphologically Panel B egg chambers at $t = 60$ min are equivalent to Panels A and C egg chambers at $t = 0$ min.

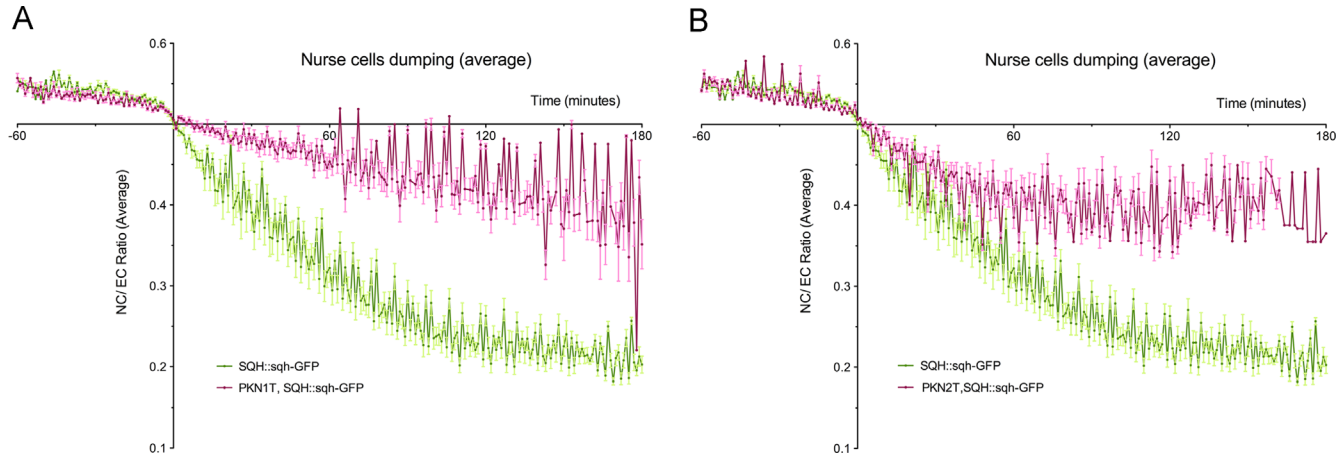

Fig. 8. Pkn is required for an efficient cytoplasm transfer rate during nurse cell dumping. *Ex-vivo* nurse cells dumping rates in control and *pkn* mutant egg chambers (see methods for more details). Time zero was defined as the first moment when the total length of the nurse cells cluster (NC)/total length of the egg chamber (EC) was equal to 0.5. (A, B) Graphs show the average NC/EC ratio before (−60 min) and after (+180 min) time zero. Control egg chambers (Sqh-GFP) are shown with a green line, whereas *pkn* mutant egg chambers (respectively: FRT42B pkn^{1T}, Sqh-GFP and FRT42B pkn^{2T}, Sqh-GFP) are shown with a purple line.

likely to provide a negative feedback loop that helps to avoid excessive contractility after local activation of Rho GTPase.

The molecular mechanism by which *Drosophila* Pkn negatively regulates MRLC phosphorylation during oogenesis is still unknown. Immunopurification experiments using a Myc-tagged Pkn have failed to identify any protein known to regulate MRLC phosphorylation (data not shown). Furthermore, liquid chromatography–mass spectrometry of Myc-Pkn imunoprecipitated protein complexes has also failed to identify any protein capable of explaining the observed phenotypes (data not shown). *pkn* mutant phenotypes during embryonic dorsal closure and wing morphogenesis are enhanced by distinct JNK signaling mutant alleles (Lu and Settleman, 1999; Sass and Ostrow, 2014). It was suggested that the Rho1-Pkn and JNK are parallel signaling pathways that "converge at some point" in their function (Lu and Settleman, 1999). Capping protein beta (Cpb) regulation of F-actin polymerization restricts JNK signaling (Fernandez et al., 2014). A strong hypomorphic allele of *cpb* (cpb^{M143}) behaved as a dominant suppressor of the *pkn* mutant short-egg phenotype. This suggests that JNK and Rho1–Pkn signaling pathways are also potentially positively related during nurse cells dumping. It was recently suggested that Pkn is required for F-actin recruitment after wound healing (Abreu-Blanco et al., 2014). This is in contrast with the dramatic F-actin accumulation we observed in egg chambers mutant for *pkn*. Although we lack any obvious explanation for such apparent difference, it might be related with tissue or context-specific functions of Pkn during development. The striking accumulation of actin–myosin cytoskeleton mostly in the central region of *pkn* mutant egg chambers suggests unknown mechanisms likely to spatially regulate nurse cells contractility during dumping. Although speculative, the most parsimonious explanation for all our results is that Pkn behaves directly or indirectly as negative regulator of Rok during nurse cells dumping. Nevertheless, we failed to identify any biochemical interaction between Pkn and Rok (data not shown). Future work will help us to elucidate the mechanism by which Pkn behaves as a negative regulator of actin–myosin activity during nurse cells dumping, and to what extent such function is conserved in other morphogenetic processes.

Acknowledgments

Both *pkn* mutant alleles were isolated in the laboratory of Ruth Lehmann. We thank our colleague Paulo Navarro Costa for discussion and suggestions that greatly improved the manuscript; Richard Hampson for manuscript editing. The work is supported by National Portuguese Funding through Grants FCT-Fundação para Ciência e Tecnologia [PTDC/SAU-BID/111796/2009, PTDC/BIA-BCM/111822/2009, PTDC/BBB-BQB/0712/2012, and PEst-OE/EQB/LA0023/2013]. T.F. had a fellowship from Fundação para Ciência e Tecnologia [SFRH/BD/37587/2007].

Appendix A. Supporting information

Supplementary data associated with this article can be found in the online version at http://dx.doi.org/10.1016/j.ydbio.2014.08.008.

References

Abreu-Blanco, M.T., et al., 2014. Coordination of Rho family GTPase activities to orchestrate cytoskeleton responses during cell wound repair. Curr. Biol. 24, 144–155.
Bastock St, R., Johnston, D., 2008. Drosophila oogenesis. Curr. Biol. 18, R1082–R1087.
Betson, M., Settleman, J., 2007. A rho-binding protein kinase C-like activity is required for the function of protein kinase N in Drosophila development. Genetics 176, 2201–2212.
Calautti, E., et al., 2002. Fyn tyrosine kinase is a downstream mediator of Rho/PRK2 function in keratinocyte cell–cell adhesion. J. Cell Biol. 156, 137–148.
Chou, T.B., Perrimon, N., 1992. Use of a yeast site-specific recombinase to produce female germline chimeras in Drosophila. Genetics 131, 643–653.
Cooper, J.A., Sept, D., 2008. New insights into mechanism and regulation of actin capping protein. Int. Rev. Cell Mol. Biol. 267, 183–206.
Dong, L.Q., et al., 2000. Phosphorylation of protein kinase N by phosphoinositide-dependent protein kinase-1 mediates insulin signals to the actin cytoskeleton. Proc. Natl. Acad. Sci. U. S. A. 97, 5089–5094.
Fernandez, B.G., et al., 2014. Drosophila actin-capping protein limits JNK activation by the Src proto-oncogene. Oncogene 33, 2027–2039.
Gardel, M.L., et al., 2004. Elastic behavior of cross-linked and bundled actin networks. Science 304, 1301–1305.
Gates, J., et al., 2009. Enabled and capping protein play important roles in shaping cell behavior during Drosophila oogenesis. Dev. Biol. 333, 90–107.
Grassie, M.E., et al., 2011. The myosin phosphatase targeting protein (MYPT) family: a regulated mechanism for achieving substrate specificity of the catalytic subunit of protein phosphatase type 1delta. Arch. Biochem. Biophys. 510, 147–159.
Guilgur, L.G., et al., 2012. Drosophila aPKC is required for mitotic spindle orientation during symmetric division of epithelial cells. Development 139, 503–513.
Ikebe, M., et al., 1988. Effects of phosphorylation of light chain residues threonine 18 and serine 19 on the properties and conformation of smooth muscle myosin. J. Biol. Chem. 263, 6432–6437.
Jacinto, A., et al., 2002. Dynamic analysis of dorsal closure in Drosophila: from genetics to cell biology. Dev. Cell. 3, 9–19.
James, R.G., et al., 2013. Protein kinase PKN1 represses Wnt/beta-Catenin signaling in human melanoma cells. J. Biol. Chem. 288, 34658–34670.
Jung, H.S., et al., 2008. Head-head and head-tail interaction: a general mechanism for switching off myosin II activity in cells. Mol. Biol. Cell 19, 3234–3242.
Kimura, K., et al., 1996. Regulation of myosin phosphatase by Rho and Rho-associated kinase (Rho-kinase). Science 273, 245–248.

Koenderink, G.H., et al., 2009. An active biopolymer network controlled by molecular motors. Proc. Natl. Acad. Sci. U. S. A. 106, 15192–15197.
Leenders, F., et al., 2004. PKN3 is required for malignant prostate cell growth downstream of activated PI 3-kinase. EMBO J. 23, 3303–3313.
Leung, T., et al., 1996. The p160 RhoA-binding kinase ROK alpha is a member of a kinase family and is involved in the reorganization of the cytoskeleton. Mol. Cell. Biol. 16, 5313–5327.
Levayer, R., Lecuit, T., 2012. Biomechanical regulation of contractility: spatial control and dynamics. Trends Cell Biol. 22, 61–81.
Lim, M.A., et al., 2004. Roles of PDK-1 and PKN in regulating cell migration and cortical actin formation of PTEN-knockout cells. Oncogene 23, 9348–9358.
Lu, Y., Settleman, J., 1999. The Drosophila Pkn protein kinase is a Rho/Rac effector target required for dorsal closure during embryogenesis. Genes Dev. 13, 1168–1180.
Mahajan-Miklos, S., Cooley, L., 1994. Intercellular cytoplasm transport during Drosophila oogenesis. Dev. Biol. 165, 336–351.
Matsumura, F., 2005. Regulation of myosin II during cytokinesis in higher eukaryotes. Trends Cell Biol. 15, 371–377.
Mizuno, T., et al., 2002. Drosophila myosin phosphatase and its role in dorsal closure. Development 129, 1215–1223.
Mopert, K., et al., 2012. Depletion of protein kinase N3 (PKN3) impairs actin and adherens junctions dynamics and attenuates endothelial cell activation. Eur. J. Cell Biol. 91, 694–705.
Morris, L.X., Spradling, A.C., 2011. Long-term live imaging provides new insight into stem cell regulation and germline-soma coordination in the Drosophila ovary. Development 138, 2207–2215.
Mukai, H., 2003. The structure and function of PKN, a protein kinase having a catalytic domain homologous to that of PKC. J. Biochem. 133, 17–27.
Mukai, H., Ono, Y., 1994. A novel protein kinase with leucine zipper-like sequences: its catalytic domain is highly homologous to that of protein kinase C. Biochem. Biophys. Res. Commun. 199, 897–904.
Nobes, C.D., Hall, A., 1995. Rho, rac, and cdc42 GTPases regulate the assembly of multimolecular focal complexes associated with actin stress fibers, lamellipodia, and filopodia. Cell 81, 53–62.
Oishi, K., et al., 1999. Identification and characterization of PKNbeta, a novel isoform of protein kinase PKN: expression and arachidonic acid dependency are different from those of PKNalpha. Biochem. Biophys. Res. Commun. 261, 808–814.
Pimenta-Marques, A., et al., 2008. Differential requirements of a mitotic acetyltransferase in somatic and germ line cells. Dev. Biol. 323, 197–206.
Prasad, M., et al., 2007. A protocol for culturing Drosophila melanogaster stage 9 egg chambers for live imaging. Nat. Protoc. 2, 2467–2473.
Quilliam, L.A., et al., 1996. Isolation of a NCK-associated kinase, PRK2, an SH3-binding protein and potential effector of Rho protein signaling. J. Biol. Chem. 271, 28772–28776.
Raghavan, S., et al., 2000. Protein phosphatase 1beta is required for the maintenance of muscle attachments. Curr. Biol. 10, 269–272.
Ridley, A.J., Hall, A., 1992. The small GTP-binding protein rho regulates the assembly of focal adhesions and actin stress fibers in response to growth factors. Cell 70, 389–399.
Royou, A., et al., 2004. Reassessing the role and dynamics of nonmuscle myosin II during furrow formation in early Drosophila embryos. Mol. Biol. Cell 15, 838–850.
Royou, A., et al., 2002. Cortical recruitment of nonmuscle myosin II in early syncytial Drosophila embryos: its role in nuclear axial expansion and its regulation by Cdc2 activity. J. Cell Biol. 158, 127–137.
Sass, G.L., Ostrow, B.D., 2014. Disruption of the protein kinase N gene of drosophila melanogaster results in the recessive delorean allele (pkndln) with a negative impact on wing morphogenesis. G3 (Bethesda) 4, 643–656.
Schmidt, A., et al., 2007. Rho GTPases regulate PRK2/PKN2 to control entry into mitosis and exit from cytokinesis. EMBO J. 26, 1624–1636.
Sellers, J.R., 2000. Myosins: a diverse superfamily. Biochim. Biophys. Acta 1496, 3–22.
St Johnston, D., 2002. The art and design of genetic screens: *Drosophila melanogaster*. Nat. Rev. Genet. 3, 176–188.
Unsal-Kacmaz, K., et al., 2012. The interaction of PKN3 with RhoC promotes malignant growth. Mol. Oncol. 6, 284–298.
Vicente-Manzanares, M., et al., 2009. Non-muscle myosin II takes centre stage in cell adhesion and migration. Nat. Rev. Mol. Cell Biol. 10, 778–790.
Vincent, S., Settleman, J., 1997. The PRK2 kinase is a potential effector target of both Rho and Rac GTPases and regulates actin cytoskeletal organization. Mol. Cell. Biol. 17, 2247–2256.
Wallace, S.W., et al., 2011. The Rho target PRK2 regulates apical junction formation in human bronchial epithelial cells. Mol. Cell. Biol. 31, 81–91.
Wheatley, S., et al., 1995. Drosophila nonmuscle myosin II is required for rapid cytoplasmic transport during oogenesis and for axial nuclear migration in early embryos. Development 121, 1937–1946.
Winter, C.G., et al., 2001. Drosophila Rho-associated kinase (Drok) links Frizzled-mediated planar cell polarity signaling to the actin cytoskeleton. Cell 105, 81–91.
Zhang, L., Ward, R.E.t., 2011. Distinct tissue distributions and subcellular localizations of differently phosphorylated forms of the myosin regulatory light chain in Drosophila. Gene Expr. Patterns 11, 93–104.